

# **HiSST: 4th International Conference on High-Speed Vehicle Science Technology** 22 -26 September 2025, Tours, France



## Design testing and thermal management of the Scramjet Hypersonic **Experimental Vehicle**

P. Roncioni <sup>1</sup>, O. Russo <sup>2\*</sup>, A. Filosa <sup>3</sup>, M. Marini <sup>4</sup>, S. Di Benedetto <sup>5</sup>, P. Natale <sup>6</sup>, G. Coppola <sup>7</sup>, F. Battista 8, G. Ranuzzi 9, M. Albano 10, F. Strauss 11

#### **Abstract**

The paper describes the main challenges involved in designing and testing the combustor of the Scramjet Hypersonic Experimental Vehicle (SHEV). The work is part of an Italian national project cofunded by the national research program PRO.R.A. and the Italian Space Agency (ASI). The comparison of experimental results from wind tunnel tests with CFD simulations will allow us to validate the numerical methodology employed. This approach can then be applied to aero-propulsive evaluation, in order to verify the scramjet engine's thrust.

Keywords: Scramjet, hypersonic, CFD, supersonic combustion, emission indexes

#### Nomenclature

ASI - Italian Space Agency CFD – Computational Fluid Dynamics CHT – Conjugate Heat Transfer CIRA – Italian Aerospace Research Centre ER - Equivalence Ratio

MFR - Mass Flow Rate SCRAMJET - Supersonic Combustion Ramjet SHEV – Scramjet Hypersonic Experimental Vehicle SSC - Second Stage Combustor

## 1. Introduction

The PRO.R.A. research program and the Italian Space Agency (ASI) are co-funding a national project on hypersonic flight aiming at developing a hypersonic demonstrator called SHEV (Scramjet Hypersonic Experimental Vehicle). The demonstrator design is based on the wave-rider concept (Fig 1) which aims to control shock waves generated during the high-speed flight for lift generation and drag reduction; in particular, the configuration studied in the EU-FP7 HEXAFLY project [1] was considered as starting point and then modified to meet the specific project objectives. The demonstrator is equipped with a scramjet engine (see Fig 2), which consists of an open inlet with a nearly elliptical capture area, where the air is compressed through oblique shock waves.

HiSST-2025-0276 Page | 1 Copyright © 2025 by author(s)

<sup>&</sup>lt;sup>1</sup> Italian Aerospace Research Centre (CIRA), Via Maiorise snc, 81043 Capua, Italy, Email: p.roncioni@cira.it

<sup>&</sup>lt;sup>2</sup> Italian Aerospace Research Centre (CIRA), Via Maiorise snc, 81043 Capua, Italy, Email: <u>o.russo@cira.it</u>

<sup>&</sup>lt;sup>3</sup> Italian Aerospace Research Centre (CIRA), Via Maiorise snc, 81043 Capua, Italy, Email: a.filosa@cira.it

<sup>&</sup>lt;sup>4</sup> Italian Aerospace Research Centre (CIRA), Via Maiorise snc, 81043 Capua, Italy, Email: m.marini@cira.it

<sup>&</sup>lt;sup>5</sup> Italian Aerospace Research Centre (CIRA), Via Maiorise snc, 81043 Capua, Italy, Email: <u>s.dibenedetto@cira.it</u>

<sup>6</sup> Italian Aerospace Research Centre (CIRA), Via Maiorise snc, 81043 Capua, Italy, Email: p.natale@cira.it

<sup>&</sup>lt;sup>7</sup> Italian Aerospace Research Centre (CIRA), Via Maiorise snc, 81043 Capua, Italy, Email: q.coppola@cira.it

<sup>8</sup> Italian Aerospace Research Centre (CIRA), Via Maiorise snc, 81043 Capua, Italy, Email: f.battista@cira.it

<sup>&</sup>lt;sup>9</sup> Italian Space Agency (ASI), Via del Politecnico snc, 00133 Rome, Italy, Email: qiuliano.ranuzzi@asi.it

<sup>10</sup> Italian Space Agency (ASI), Via del Politecnico snc, 00133 Rome, Italy, Email: marta.albano@asi.it

<sup>&</sup>lt;sup>11</sup> DLR, Langer Grund, D-74239 Hardthausen, Germany, Email: friedolin.strauss@dlr.de

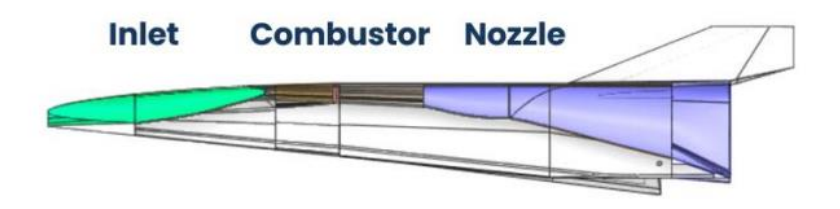


Fig 1. Demonstrator external configuration.

The flow then enters the diverging combustor where the fuel is injected, mixed with the air and ignited to produce thrust. The combustor has also an elliptical shape with a cross-section that progressively expands along its length. Hydrogen gas is used as fuel and is injected through two semi-struts located at the beginning of the combustor, supplying 65% of the total fuel mass flow rate, and a full-strut nearly at mid of the combustor for the remaining 35%.

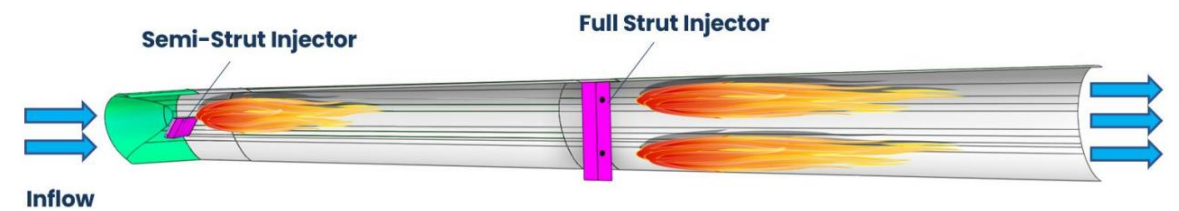
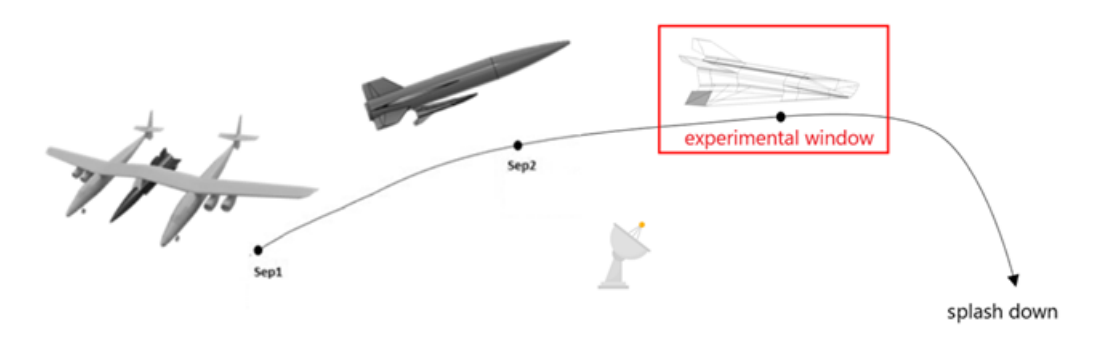


Fig 2. Scramjet combustor internal configuration.

#### 1.1. Mission Scenario

The preliminary mission scenario reported in Fig 3 involves the vehicle to be launched from an aircraft carrier and accelerated by a solid rocket booster with aerodynamic control capabilities to reach a target speed Mach number between 6-8 and an altitude ranging from 27 to 32 km. At that stage, the demonstrator is released, and the scramjet engine is turned on, with the objective of maintaining a controlled and stable flight for approximately 10 seconds [2].



**Fig 3.** Mission scenario.

## 2. Experimental firing test: limitations and updates

An experimental firing test campaign is planned and will be potentially conducted at DLR's M11.1 propulsion facility at Lampoldshausen. The campaign will concentrate solely on the scramjet combustor, aiming to evaluate its performance and to verify that a stable, spontaneous combustion occurs without the aid of any electrical ignition device. This will also serve to validate the numerical predictions previously carried out [3]. The DLR M11.1 facility consists of an air vitiator facility in a direct-connect

configuration, and it is identified as suitable option to validate the combustor. The test bed (see Fig 4) is equipped with a series of 11 hydrogen-oxygen pre-burners which heat up pressurized air. Makeup oxygen is added after the combustion process to reestablish the chemical composition of ambient air. The facility is able to generate a subsonic flow with a mass flow rate of up to 5 kg/s, a total temperature of 1500 K and a total pressure of up to 25 bar. [4]

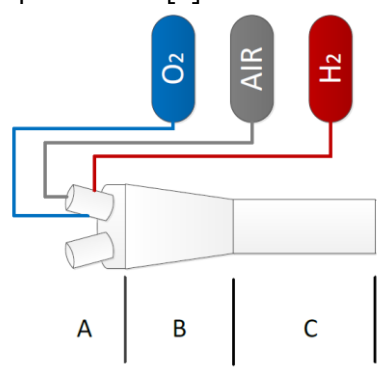


Fig 4. DLR M11.1 facility sketch.

A brief comprehensive CFD analysis was carried out by using ANSYS-FLUENT® for the full-scale combustor considering the facility's operating limits in terms of mass flow rate, total temperature, and total pressure, to preliminary assess the combustion process under these conditions. The numerical models used were the SST-k $\omega$  model for the turbulence and the EDC combustion model with a chemical mechanism for hydrogen-air mixture. Each value reported in the contours and plot is normalized with respect to its reference values.

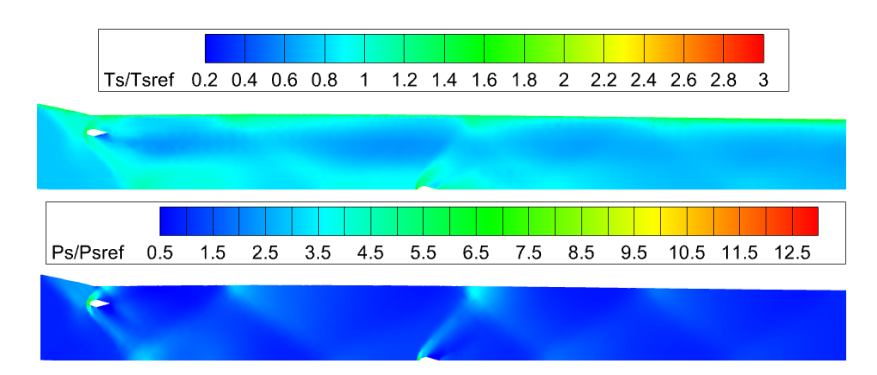


Fig 5. Temperature and pressure normalized contour of the second optimized SHEV combustor.

Although the facility meets CIRA requirements in terms of mass flow rate and total pressure, a fairly severe restriction is the maximum total temperature of 1500K, which makes the air-hydrogen mixture difficult to auto-ignite and to sustain combustion as reported in Fig 5. To overcome this issue and to allow scramjet combustion testing, CIRA designed an additional component to be integrated into the already existing DLR propulsion test rig: a second stage combustor that rises the total temperature up to 2000 K and interfaces directly with the facility's outlet.

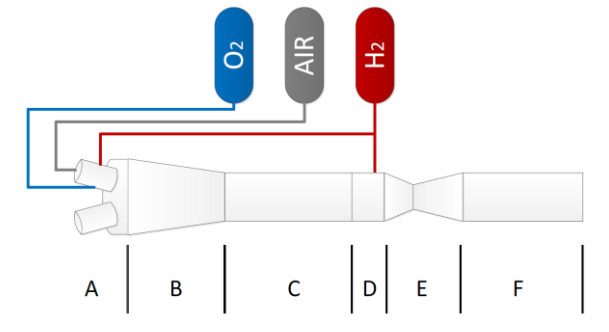
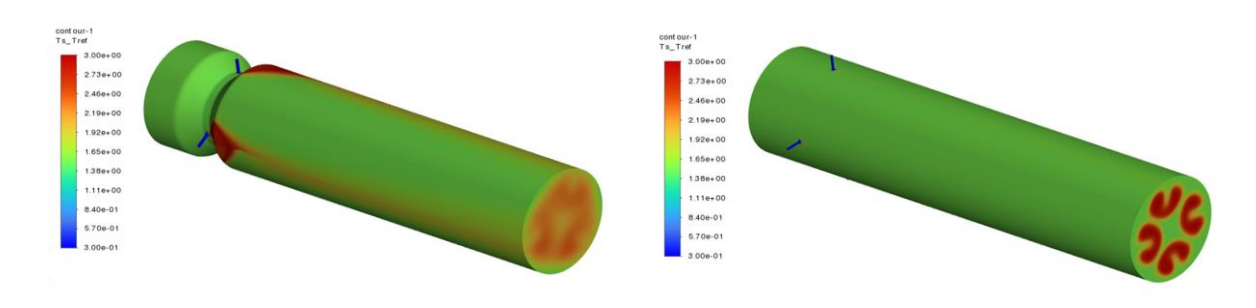


Fig 6. DLR facility bench scheme for SHEV combustor testing.

A possible solution for the second stage combustor is shown in Fig 7. It involves the use of appropriately staggered fuel injectors with a geometry restriction, designed to promote a good level of homogenization for the temperature distribution at the outlet. However, according the numerical simulations this setup requires a particular management of the wall heat flux. To reduce the thermal stress on the exposed surfaces and to improve the reliability of the system during the tests, an alternative solution is currently being developed, which removes the restriction and increases the number of injectors from three to four. While this modification reduces the wall heat flux, it also leads to a decrease in the temperature homogenization, which may affect negatively the combustion performance and the overall efficiency



**Fig 7.** Possible solutions for the second stage combustor. Reference (left) and Alternative with 4-injector (right).

The non-uniformity of the 4-injector configuration is evident in the scatter plots Fig 8, which illustrate the radial temperature distribution at the combustor outlet. In the reference configuration, the data points are tightly clustered around the mean temperature curve, indicating good radial uniformity. In contrast, the 4-injector case without restrictions (U = 0.772) exhibits a much broader spread, especially near the walls and centerline, evidencing significant non-uniformity in the outlet temperature profile.

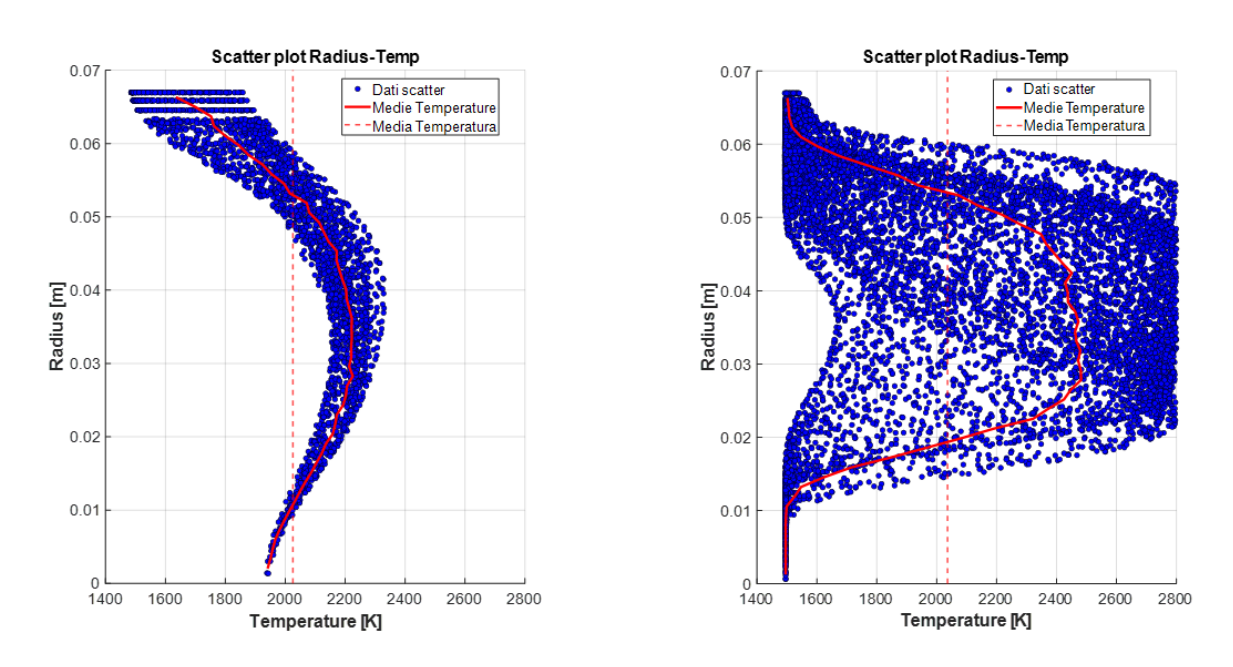


**Fig 8.** Scatter Plot of the Temperature distribution at the outlet.

## 2.1. Nozzle design and scramjet integration

The Nozzle adapter is another component designed by CIRA to accelerate the flow from subsonic to supersonic conditions. It connects the second-stage combustor, which raises the total temperature up to 2000K to sustain stable combustion, and the scramjet combustor. The nozzle adapter also provides the geometric transition in the converging section, adapting the circular cross-section of the second-stage combustor to the elliptical shape of the scramjet combustor inlet. Its elliptical outlet is shaped to provide a smooth fluid-dynamic interface between the adapter and the combustor.

The semi-major axis of the divergent portion is designed using the Method of Characteristics (MoC) [5], while the curve for the semi-minor axis was scaled proportionally for the sake of geometrical consistency. A spline curve is used to generate to whole convergent sector of the nozzle, hence giving a smooth and effective geometry transition from the inlet to the throat.

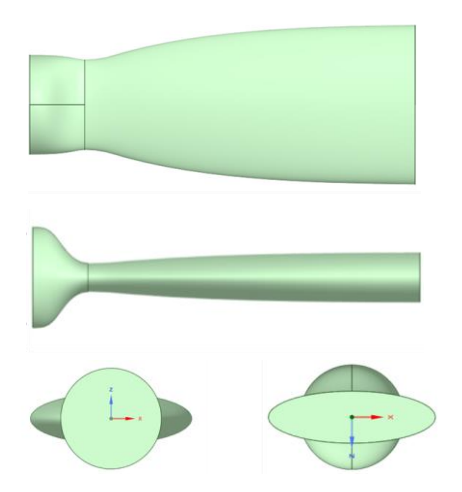


Fig 9. Bell nozzle shape.

To simplify the CFD analysis and reduce the computational effort, CFD simulations were carried out considering only the nozzle adapter and the scramjet engine.



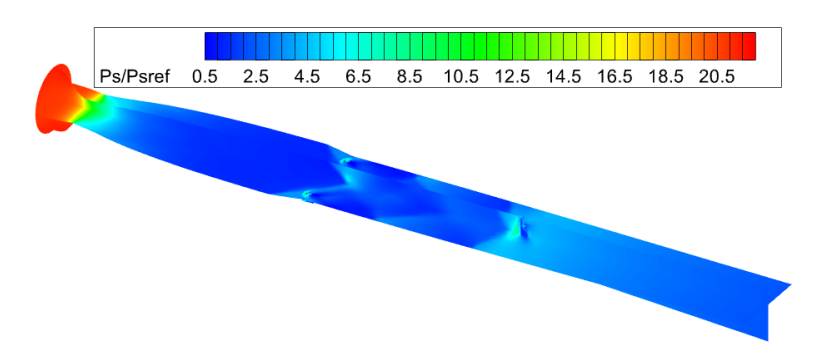
Fig 10. Bell nozzle shape with optimized combustor.

A full configuration was modelled employing an unstructured grid consisting of 7-million cells. The tetrahedral mesh also incorporates a prism layer to accurately model the flow features near the walls.

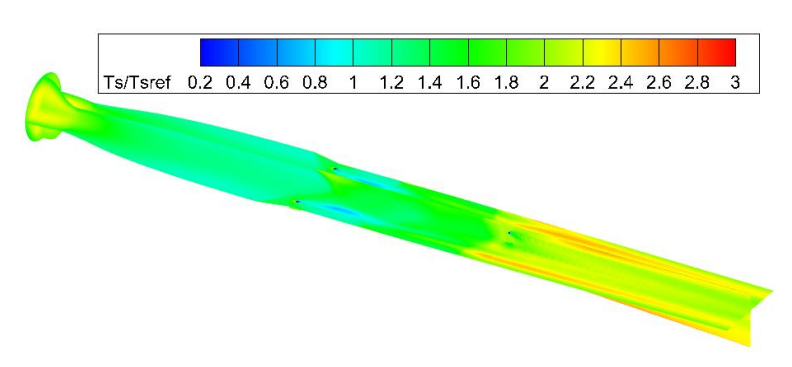


Fig 11. Computational mesh for the bell nozzle configuration including the optimized combustor.

The outflow conditions from the two possible solutions of the second-stage combustor Fig 7 were applied as discrete point values at the nozzle inlet.



**Fig 12.** Static pressure contour with inlet conditions from the first solution for the second-stage combustor.



**Fig 13.** Static temperature contour with inlet conditions from the first solution for the second-stage combustor.

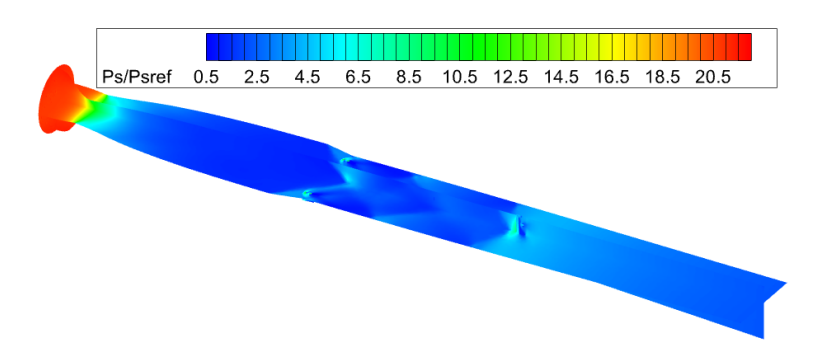


**Fig 14.** Static pressure contour with inlet conditions from the second solution for the second-stage combustor.

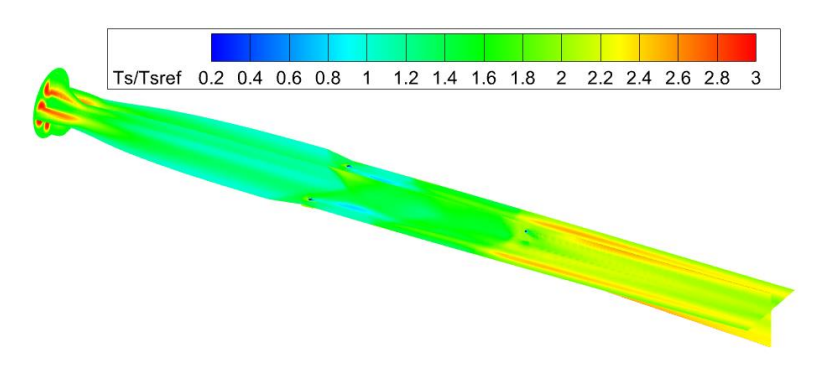


**Fig 15.** Static temperature with inlet conditions from the second solution of the second-stage combustor.

The static pressure and temperature contours plots Fig 12 - Fig 15 for both possibilities of the second stage combustor show a high degree of similarity, as further confirmed by Fig 16 - Fig 18. This suggests that, regardless of the specific solution used for the second-stage combustor, the nozzle ensures a

homogeneous supersonic flow of the mixture before it enters the combustion chamber, a fundamental aspect to optimize the performance of the overall system. Therefore, the second solution without restriction for the second stage combustor represents a suitable and reliable option for managing thermal distribution, without relying on cooling systems.

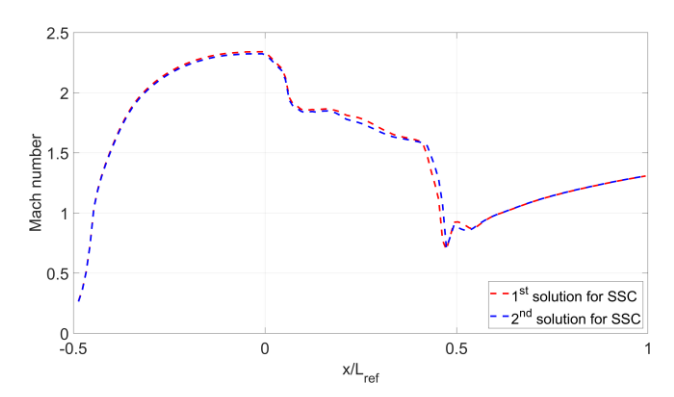


**Fig 16.** Comparison of averaged Mach number profiles for different output from SSC along the NozzScram.

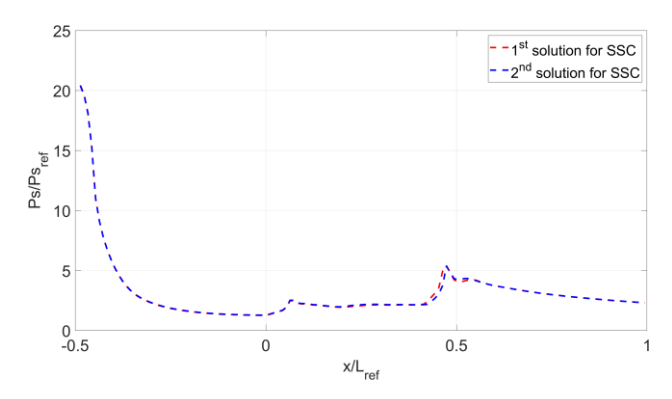


**Fig 17.** Comparison of averaged static pressure profiles for different output from SSC along the NozzScram.

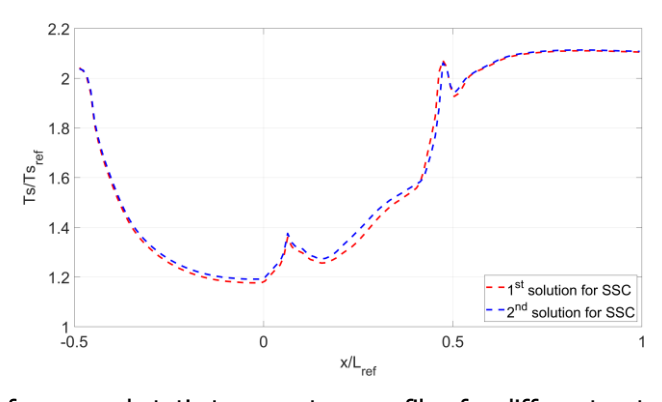


**Fig 18.** Comparison of averaged static temperature profiles for different output from SSC along the NozzScram.

In both complete system configurations, the flame position is located near the full-strut. This effect could be attributed to the value of the hydrogen mass flow rate, which is based on the pure air at the inlet and is consistent with the flight condition (ER = 1). Considering the overall system and the presence of vitiated air upstream of the nozzle due to pre-combustion, the mixture composition is altered so that the global equivalence ratio into combustor reaches 1.3, indicating a fuel-rich mixture.

## 3. Cooling system description

The nozzle adapter and the scramjet combustor are subjected to intense wall heat fluxes. In the nozzle adapter, the throat region results in high heat flux due to the sonic condition and the strong temperature gradients, while in the scramjet combustor, the combination of supersonic flow and the combustion process significantly increases the convective heat transfer to the walls. Hence, a detailed thermal analysis is needed for these two components to try to limit the wall temperature during the operation and to ensure fluid-dynamic performance.

## 3.1. Cooling system for nozzle adapter

A dedicated water-cooled system has been designed to protect the internal wall of the nozzle adapter. This device is intended mainly for the firing test campaign to reduce the possibility of failure due to material degradation under high thermal loads. The cooling system consists of a series of circular microchannels, in which liquid water flows to absorb heat. These channels are evenly spaced along the azimuthal direction and embedded in the 10 mm thick solid walls of the nozzle adapter. To enhance coolant distribution across the surface, the channels bifurcate approximately halfway along the divergent section. Each channel has a circular cross-section with a diameter of 5 mm. The internal layout of the cooling system for the nozzle device is shown Fig 19.

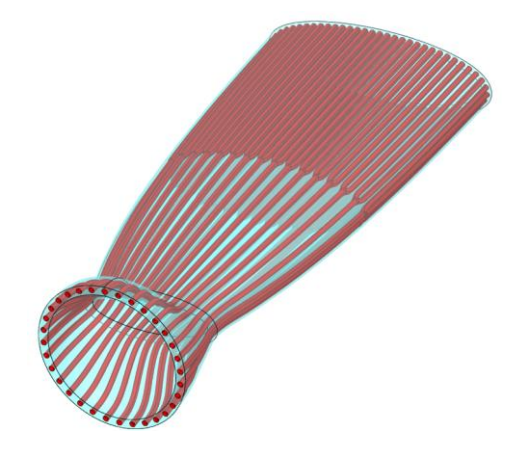


Fig 19. Nozzle Adapter: Cooling system design.

Conjugate Heat Transfer (CHT) simulations were performed to accurately capture the thermal interaction between the fluid and solid domains. The computational model consists of three distinct regions, which are simultaneously resolved by the commercial code ANSYS FLUENT [6]: the hot gas region, the solid wall, and the cooling channel. FLUENT computes the temperature field for both the fluids (hot gas and the coolant) as well as the heat conduction in the solid material. More details on the cooling approach can be found in [9].

Fig 20 shows the computational mesh for the nozzle with its cooling jacket and internal channels. The gas domain is discretized using a polyhedral mesh with a boundary layer thickness of  $5\times10^{-5}$  m, ensuring a y<sup>+</sup>  $\approx$  100 at the throat region. The coolant domain within the cooling channels adopts a tetrahedral mesh with a characteristic element size of 1 mm, and a boundary layer near the walls with a first cell height of  $1.5\times10^{-5}$  m. The solid domain (nozzle wall and cooling jacket) is meshed with a size of 1.5 mm on the outer surfaces and 1 mm around the cooling channels, allowing accurate thermal conduction modeling.

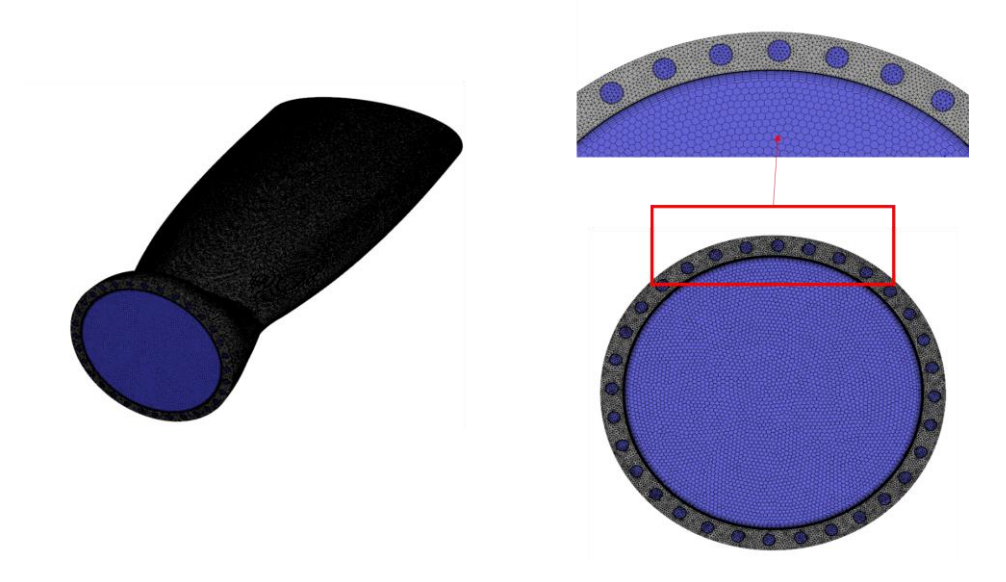
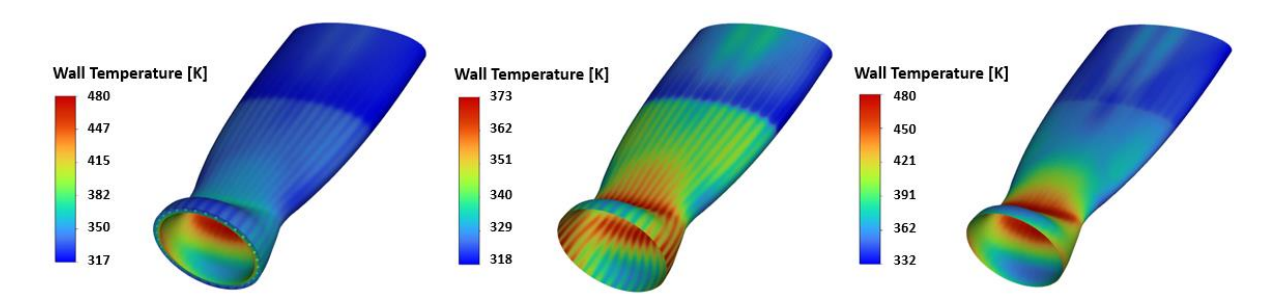


Fig 20. Computational mesh for the Nozzle Adapter.

The numerical results for the solid region are indicated in Fig 21. It shows the temperature distribution on the internal wall, within the solid domain, and on the external wall of the nozzle. The results are obtained from the CHT simulation imposing a coolant mass flow rate of 5kg/s. The internal wall surface is in direct contact with the hot gas and shows a maximum temperature of approximately 470 K in the throat region, where the wall heat flux is the most intense due to the combination of high convective heat transfer and elevated gas temperatures. This temperature peak, which is below the material limit, results from the combined effect of the intense heating from the hot gas and the simultaneous cooling from the coolant, which absorbs part of the heat cooling down the wall.

The elliptical shape of the throat leads also to non-uniform wall heat transfer distribution. Although it remains, in absolute terms, the most critical region, the maximum thermal load is not evenly distributed and occurs along the semi-minor axis, where the curvature is tighter. The divergent section, due to the flow expansion which leads to a reduction in the gas temperature, appears less thermally stressed compared to the convergent part.

The external wall is significantly cooler than the internal one. In the simulation, it is modeled as adiabatic, neglecting any external heat transfer and focusing the thermal analysis only on the internal domain.



**Fig 21.** Nozzle Adapter - Solid Region Results: Temperature distribution in the solid wall and on the internal wall.

#### 3.2. Cooling system for scramjet

This cooling system is composed of 64 circular channels with constant cross-sections, equally spaced and embedded in the solid wall. Each channel measures 5 mm in diameter, while the wall itself is 10 mm thick. The channels are straight and follow the geometry of the inner surface. In this preliminary design, which does not account for injector feeding space or the added instrumentation for thermocouples and pressure transducers, the goal is to estimate both the wall temperature and the water mass flow rate necessary for effective cooling. Fig 22 illustrates the cooling configuration employed for the scramjet combustor.

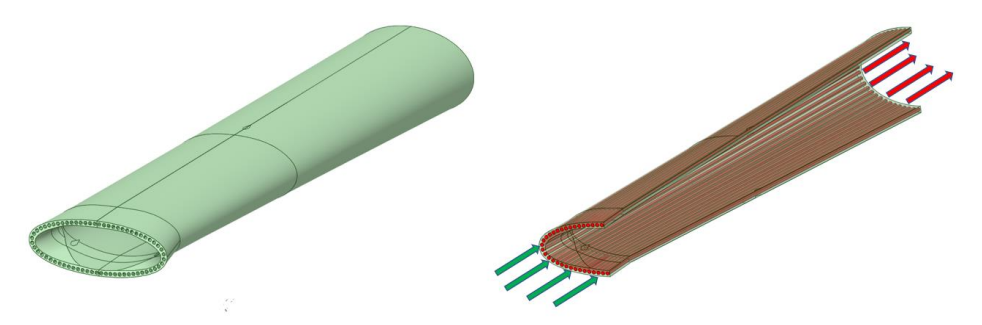


Fig 22. Scramjet Combustor. Cooling system design.

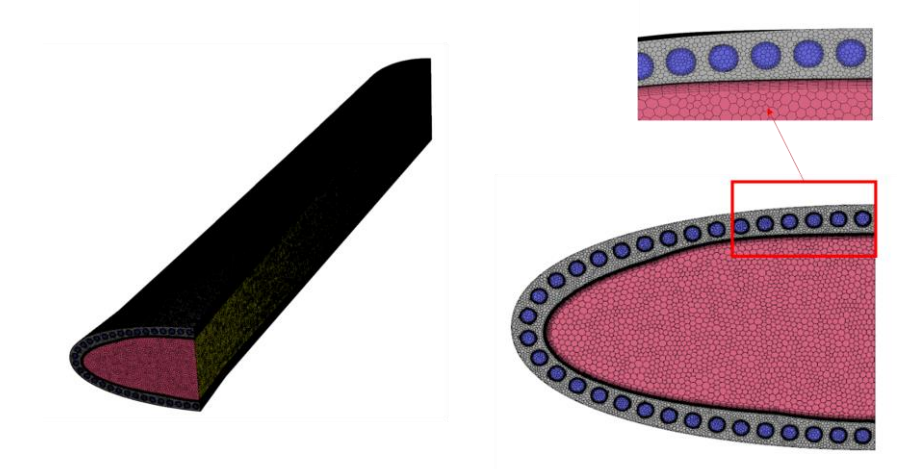
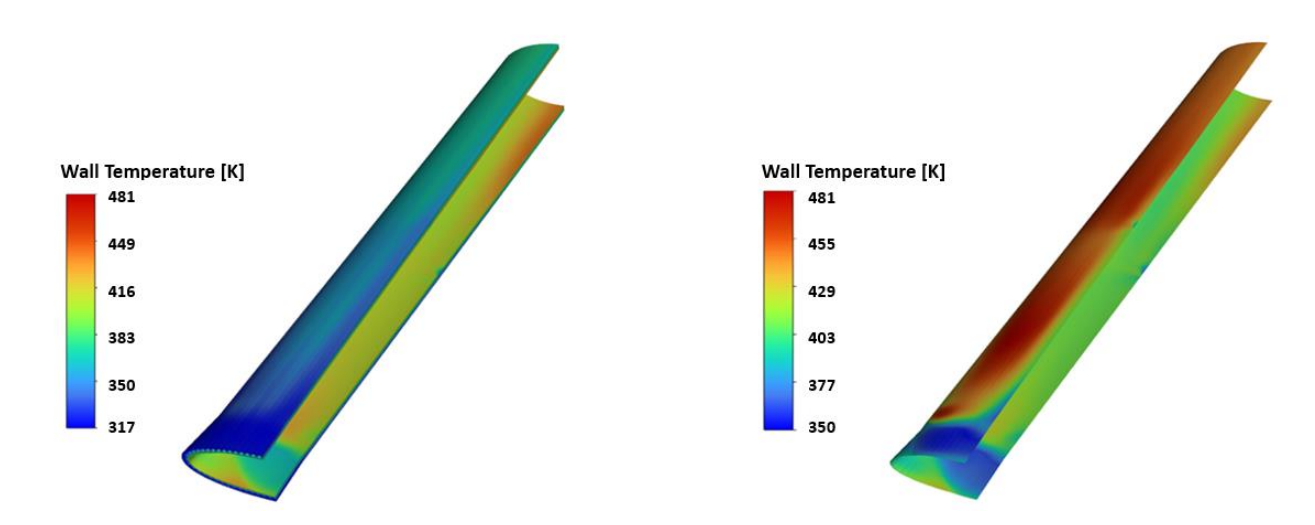


Fig 23. Computational mesh for the Scramjet Engine.

Fig 23 shows the mesh for the scramjet geometry, including the internal gas domain, solid wall, and cooling channels. All regions were initially discretized with a tetrahedral mesh, then converted to polyhedral elements within ANSYS Fluent to improve numerical stability and reduce computational time. The meshing strategy and resolution closely follow the approach adopted for the nozzle case:

Fig 24 presents the wall temperature distribution obtained from the conjugate heat transfer (CHT) simulation of the scramjet combustor. The left image illustrates the temperature field inside the solid domain, and the wall temperature distribution on the outer wall. Similar for the nozzle adapter case, this wall is treated as adiabatic in simulation and shows a significantly lower temperature profile than the internal wall. The inner surface, in contrast, is exposed to the hot gas stream and to the intense heat generated by the combustion process. The auto-ignition of the hydrogen originates downstream the semi-strut injector with a lifted flame which impinges directly on the upper part of the wall, leading to a localized region of high heat flux. This effect generates a non-uniform pattern for the wall temperature: the hottest spot is localized in the impingement region, where high convective heat transfer occurs. Conversely, the lower wall remains relatively cooler, since it experiences a limited interaction with the hot combustion gases. The maximum temperature on the internal wall surface

reaches approximately 480K which is well below the material limit and indicates a safe operating condition with the coolant mass flow rate considered in the simulation.



**Fig 24.** Scramjet Combustor - Solid Region Results: Temperature distribution in the solid wall and on the internal wall.

#### 4. Conclusions

The experimental validation of the scramjet combustor represents a crucial step to compare the CFD data with real measurements and evaluate the behavior of the SHEV combustor under realistic operating conditions. These tests will allow us to identify any discrepancies between the numerical model and the experimental tests. The CFD analyses conducted so far have highlighted some critical issues related to the thermodynamic conditions available in the current DLR facility. To support the firing test campaign of the SHEV scramjet combustor at the DLR M11.1 facility, two additional components were developed to guarantee the ignition and a stable supersonic combustion: a second-stage combustor that increases the flow's total temperature and a nozzle adapter that accelerates the flow to supersonic conditions. Because the thermal loads on the second-stage combustor are moderate, it does not require active cooling. In contrast, the nozzle adapter and the scramjet combustor both experience high heat flux and therefore demand dedicated cooling systems. In particular, the nozzle adapter integrates 32 circular micro-channels embedded in the wall, which bifurcate around the midpoint of the divergent section to optimize coolant distribution. Meanwhile, the scramjet combustor employs a similar layout but doubles the number of channels to 64, thereby boosting the overall heat removal capacity.

In conclusion, the use of the second-stage combustor is crucial for achieving the optimal thermal condition necessary to sustain a supersonic combustion into the combustor of SHEV. Furthermore, as highlighted by CFD simulations, dedicated cooling systems for nozzle adapter and scramjet combustor are essential for maintaining material temperatures within acceptable limits.

#### References

- [1] Steelant, J. et al.: Conceptual Design of the High-Speed Propelled Experimental Flight Test Vehicle HEXAFLY. AIAA-2015-3539, 20th AIAA International Space Planes and Hypersonic Systems and Technologies Conference, 2015, Glasgow, Scotland, U.K.
- [2] M. Marini, S. Di Benedetto, P. Roncioni, O. Russo, F. Cascone, G. Di Lorenzo, P. Natale, P. Vernillo, A. Vitale, M. Albano, R. Bertacin, "Technological challenges of the design of a SCRAMJET hypersonic vehicle and its flight mission", IAC, 2024, Milan.

- [3] O. Russo, A. Filosa, M. Marini, P. Roncioni, S. Di Benedetto, P. Natale, G. Coppola, F. Battista, F. Strauss, M. Albano, G. Ranuzzi, "Design and Testing challenge of the Scramjet Hypersonic Experimental Vehicle", 3rd International Conference on Flight vehicles, Aerothermodynamics and Re-entry, FAR 2025, Archaeon, France.
- [4] Test bench complex M11, DLR site Lampoldshausen, <a href="https://www.dlr.de">https://www.dlr.de</a>.
- [5] Guentert, E. C., Neumann, H. E. "Design of Axisymmetric Exhaust Nozzles by Method of Characteristics Incorporating a Variable Isentropic Exponent". 1959. Stati Uniti: National Aeronautics and Space Administration.
- [6] Fluent Theory Guide 2023 R1.
- [7] G. Saccone, P. Natale, M. Marini, L. Cutrone, "Hydrogen/Air Supersonic Combustion Modelling and Validation for Scramjet Applications", Journal of Fluid Flow, Heat and Mass Transfer (JFFHMT), doi: 10.11159/jffhmt.2022.017.
- [8] R. Citatella, M. Ferraiuolo, M. Perrella, V. Giannella, "Thermostructural Numerical Analysis of the Thrust Chamber of a Liquid Propellant Rocket Engine", Materials 2022, 15, 5427.
- [9] A. Filosa, O.Russo, P. Natale, G. Coppola, M. Marini, P. Roncioni, S. Di Benedetto, F. Battista, F. Strauss, M. Albano, G. Ranuzzi, "Cooling system design for the Scramjet Hypersonic Experimental Vehicle", 11th European Conference for AeroSpace Sciences (EUCASS) 30th June to 4th July 2025, Rome, Italy